

# Direct Determination of Expansion History Using Redshift Distortions

Yong-Seon Song

*Korea Astronomy and Space Science Institute, Daejeon 305-348, R. Korea*

(Dated: October 25, 2012)

We investigate direct determination of expansion history using redshift distortions without plugging into detailed cosmological parameters. The observed spectra in redshift space include a mixture of information: fluctuations of density-density and velocity-velocity spectra, and distance measures of perpendicular and parallel components to the line of sight. Unfortunately it is hard to measure all the components simultaneously without any specific prior assumption. Common prior assumptions include a linear/quasi-linear model of redshift distortions or a model for the shape of the power spectra, which eventually breaks down on small scales at later epochs where nonlinear structure formation disturbs coherent growth. The degeneracy breaking between the effect of cosmic distances and redshift distortions for example depends on the prior we assume. As an alternative approach is to utilize the cosmological principle inscribed in the heart of the Friedmann–Lematre–Robertson–Walker (hereafter FLRW) universe, that is, the specific relation between the angular diameter distance and the Hubble parameter, in this degeneracy breaking. We show that utilizing this FLRW prior early in the step of distinguishing the distance effect from redshift distortions help us improve the detectability of power spectra and distance measures with no leaning on combination of other experiments.

PACS numbers: draft

## I. INTRODUCTION

Fundamental cosmological observables of the universe are cosmic expansion, large scale structure formation and curvature of space. Those are key tracers of past, present and future of the universe. Cosmic expansion is defined by the expansion of the distance among cosmological objects of the universe with time. History of the universe is known by this expansion rate at each epoch [1]. The universe at large scale appears as a compilation of swiss cheese–like bubbles bordered by filaments of galaxies. This contemporary spatial distribution is clearly observable in a three dimensional reconstruction of the spectroscopy wide–deep survey [2]. The fate of the universe is determined by the global shape of space. Spatial manifold of the universe appears compact or non–compact without boundary [3]. Consistency of those key observables with predictions of known physical sciences on the earth will be an evidence of existence of the Friedmann–Lematre–Robertson–Walker (hereafter FLRW) universe.

Discovery of metric expansion revolutionized our understanding of the universe. The metric expansion is successfully modeled by FLRW model based upon the cosmological principle. The cosmological principle is a philosophical statement that all properties of the universe are viewed the same for all observers on a sufficiently large scale. However, the first evidence of cosmic acceleration in 1998 [4, 5] brought an issue of inconsistency between observables of FLRW universe and predictions of physical sciences. A prime goal of precision cosmology in next decades is to provide cosmological observables in a theoretical model independent way for a fair judgement of confirmation or exclusion. In order words, cosmic observation should be unplugged from our prior knowledge of underlying sciences. We investigate methods to probe

fundamental cosmological observables without plugging into theoretical models described by detailed cosmological parameters.

The full history of cosmic expansion can be reconstructed using galaxy redshift surveys. Despite the enriched nonlinear structures, the zero-th order description of our current universe is homogeneous and isotropic over sufficiently large scales [6–16]. The measured spatial distribution of galaxies is determined by the density fluctuations and the coherent peculiar velocities of galaxies. Even though we expect the clustering of galaxies in real space to have no preferred direction, galaxy maps produced by estimating distances from redshifts obtained in spectroscopic surveys reveal an anisotropic galaxy distribution. The anisotropies arise because galaxy recession velocities, from which distances are inferred, include components from both the Hubble flow and peculiar velocities driven by the clustering of matter. Measurements of the anisotropies allow constraints to be placed on the rate of growth of clustering and Hubble flow along the line of sight [17–38].

In practice, ‘referenced’ spectra of redshift distortions are observed in fiducial coordinates, instead of true spectra. Cosmological parameters are commonly applied to project measured ‘referenced’ spectra into ‘best fit’ spectra. Those ‘best fit’ spectra will be genuine only if underlying theoretical models are true. But cosmological observables should be provided *a priori* without theoretical models to be tested. To begin with, we would like to answer basic questions in FLRW universe; what is expansion rate at each epoch, what are spectra of large scale structure, and what is global curvature of the space. We would not jump into theoretical issues of cosmic acceleration; what is nature of dark energy, and what is a cosmological measure of Einstein’s gravity.

The observed spectra in redshift space not only depend

on fluctuations of density & velocity fields but also depend on distance measures of perpendicular & parallel components to the line of sight [39–44]. Unfortunately, those are not simultaneously decomposed out of redshift distortions in precision due to high degeneracy. We propose a couple of approaches to break the degeneracy among observables. The first approach is an easier way but less model-independent, and the second approach is a harder way but more model-independent.

First approach, we can, in principle, resolve this problem if we understand the shape of the power spectrum precisely. In the context of standard cosmology, the shape of spectra is determined before the last scattering surface, and in linear theory, it evolves coherently through all scales. In this case, the shape of spectra is determined by CMB experiments, both coherent growth functions of density & velocity and distance measures can be determined separately in precision using the standard ruler test or Alcock-Paczynski test [45]. Unfortunately, this ansatz is not applicable for a specific theoretical model of cosmic acceleration in which structure formation does not grow coherently at later epochs, i.e. the determined shape of spectra has been altered since last scattering surface [46–48].

Second approach, we propose an alternative method to make measurements with assuming theoretical prior as minimal as possible. In FLRW universe, the perpendicular and the parallel components can be unified based upon the spartial homogeneity. Instead of making additional theoretical antsatz, we propose the configuration of spectroscopic wide–deep field survey to be fully tomographic, i.e., composed of a series of redshift bins, over a certain range of redshift. If this observational constraint is satisfied, there is no further need for us to assume theoretical prior more than FLRW universe. We find that both power spectra and distance measures are simultaneously measurable without any assistance of other experiments. Remarkably, the expansion history of Hubble flow is measured well within a couple of percentage precision at each redshift.

We summarize the layout of this paper. In section II, probing distance measures are presented. In section III, model independent observation of spectra is presented. In section IV, remaining issues are discussed.

## II. DETERMINATION OF DISTANCE MEASURES

The observed galaxy–galaxy correlation in redshift space depends on fluctuations of density & velocity fields and distance measures of perpendicular & parallel components to the line of sight. The perpendicular component of distance measures is represented by the angular diameter distance  $D_A$ , and the parallel component is represented by the inverse of Hubble flow  $H^{-1}$  at each given redshift. The linear response of the observed power spectra to the variation of distance measures is studied

in detail in this section. In the following subsections, we present various methods to probe distance measures out of the observed spectra. The future tomographic wide–deep survey from  $z = 0$  to 2 is assumed through this paper. Fiducial cosmology model is  $\Lambda$ CDM universe with cosmological parameters of ( $\Omega_m = 0.24$ ,  $\Omega_k = 0$ ,  $h = 0.73$ ,  $A_S^2 = 2.41 \times 10^{-9}$ ,  $n_S = 0.96$ ).

### A. Components of observed galaxy power spectra

An observed galaxy power spectrum  $\tilde{P}(k, \mu, z)$  in redshift space is commonly modeled as [49] over  $k < 0.1 h \text{ Mpc}^{-1}$ ,

$$\tilde{P}(k, \mu, z) = P_{gg}(k, z) + 2\mu^2 P_{g\Theta}(k, z) + \mu^4 P_{\Theta\Theta}(k, z),$$

where the subscripts  $g$  and  $\Theta$  denote the inhomogeneity of galaxy number density and the divergence of peculiar velocity measured in the unit of  $aH$ . Power spectra  $P_{gg}$ ,  $P_{g\Theta}$  and  $P_{\Theta\Theta}$  correspond to components of fluctuations of density and velocity fields. The subscript  $g$  denotes perturbations of galaxy distribution. Galaxy number over-density  $\delta_g(k, z)$  is in general biased relative to mass fluctuations and assumed to be  $\delta_g(k, z) = b(k, z)\delta_m(k, z)$ . The fiducial value of  $b$  is assumed to be  $b = 1$  in the manuscript.

The observed spectra are transformed by variation of distance measures through correspondent coordinate components in Fourier space. With the plane wave approximation,  $k$  and  $\mu$  are given by  $k_{\perp}$  and  $k_{\parallel}$  as,

$$\begin{aligned} k &= \sqrt{k_{\perp}^2 + k_{\parallel}^2} \\ \mu &= k_{\parallel}/k. \end{aligned} \quad (1)$$

Given the observational quantities, such as  $k_{\perp}D_A$  (i.e., an angular scale) and  $k_{\parallel}H^{-1}$  (i.e., a scale along redshift), different distance measures ( $D_A$  and  $H^{-1}$ ) result in a feature of power spectra in a different wavenumber  $k_{\perp}$  and  $k_{\parallel}$ . When we have a prior information on the location of a feature in  $k_{\perp}$  and  $k_{\parallel}$ , we then can determine  $D_A$  and  $H^{-1}$ .

### B. Dependence of $\tilde{P}$ on distance measures

Anisotropy of redshift distortions gives us an opportunity to probe  $D_A$  and  $H^{-1}$  separately. The mechanism of simultaneous determination is explained in this subsection.

Decomposition of  $P_{gg}$  and  $P_{\Theta\Theta}$  out of  $\tilde{P}$  was studied previously, when  $D_A$  and  $H^{-1}$  are assumed to be well-known [23].  $P_{gg}$  spectra are precisely decomposed at  $\mu \rightarrow 0$ , and  $P_{\Theta\Theta}$  spectra are decomposed by running of  $\tilde{P}$  on  $\mu$  coordinate. Here we are interested in the reverse case. We study decomposition of  $D_A$  and  $H^{-1}$  out of  $\tilde{P}$ , when spectra of  $P_{gg}$  and  $P_{\Theta\Theta}$  are fixed.

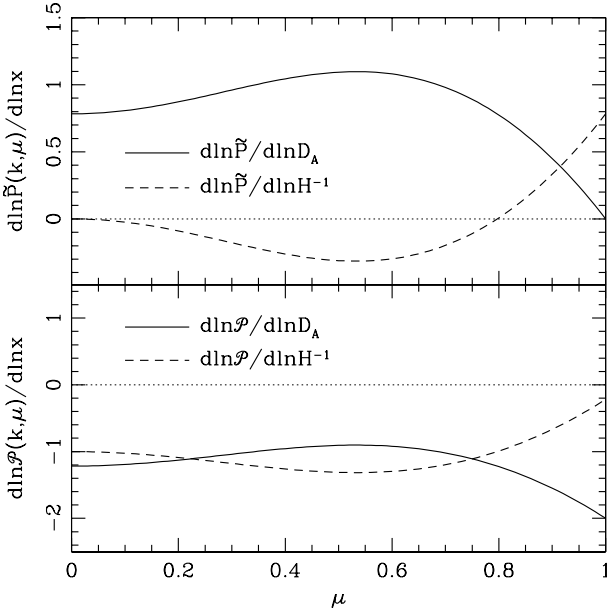


FIG. 1: (Top panel) Derivatives of  $\tilde{P}$  in terms of distance measures of  $D_A$  and  $H^{-1}$  are presented with given  $k = 0.05 h \text{Mpc}^{-1}$  and  $z = 1$ . Solid and dash curves represent derivatives of  $\tilde{P}$  in terms of  $D_A$  and  $H^{-1}$  respectively. (Bottom panel) Derivatives of  $\mathcal{P}$  in terms of distance measures of  $D_A$  and  $H^{-1}$  are presented. Solid and dash curves represent derivatives of  $\mathcal{P}$  in terms of  $D_A$  and  $H^{-1}$  respectively.

Logarithmic derivative of  $\tilde{P}$  in terms of  $D_A$  is given by,

$$\begin{aligned} \frac{d \ln \tilde{P}(k, \mu)}{d \ln D_A} &= -(1 - \mu^2) \frac{d \ln \tilde{P}(k, \mu)}{d \ln k} \\ &+ 4\mu^2(1 - \mu^2) \frac{P_{g\Theta}(k) + \mu^2 P_{\Theta\Theta}(k)}{\tilde{P}(k, \mu)}, \end{aligned} \quad (2)$$

where  $d \ln \tilde{P} / d \ln k$  is,

$$\frac{d \ln \tilde{P}}{d \ln k} = \frac{d \ln P_{gg}}{d \ln k} + 2\mu^2 \frac{d \ln P_{g\Theta}}{d \ln k} + \mu^4 \frac{d \ln P_{\Theta\Theta}}{d \ln k}.$$

Derivative of  $d \ln \tilde{P}(k, \mu) / d \ln D_A$  maximizes at  $\mu \rightarrow 0$ , and vanishes at  $\mu \rightarrow 1$ . We present it graphically in Fig. 1 with given scale of  $k = 0.05 h \text{Mpc}^{-1}$  and redshift of  $z = 1$ . Solid curve in the top panel of Fig. 1 represents the derivative in terms of  $D_A$ . It is reasonable that correlation pairs along the line of sight are unchanged by variation of perpendicular component of distance measures.

Logarithmic derivative of  $\tilde{P}$  in terms of  $H^{-1}$  is given by,

$$\begin{aligned} \frac{d \ln \tilde{P}(k, \mu)}{d \ln H^{-1}} &= -\mu^2 \frac{d \ln \tilde{P}(k, \mu)}{d \ln k} \\ &- 4\mu^2(1 - \mu^2) \frac{P_{g\Theta}(k) + \mu^2 P_{\Theta\Theta}(k)}{\tilde{P}(k, \mu)}. \end{aligned} \quad (3)$$

Derivative of  $d \ln \tilde{P}(k, \mu) / d \ln H^{-1}$  vanishes at  $\mu \rightarrow 0$ , and maximizes at  $\mu \rightarrow 1$ . It is opposite to the derivative

of  $d \ln \tilde{P}(k, \mu) / d \ln D_A$ . Dash curve in the top panel of Fig. 1 represents the derivative in terms of  $H^{-1}$ .

We observe orthogonal behavior of  $\tilde{P}$  to the variation of  $D_A$  and  $H^{-1}$ . If spectra of  $P_{gg}$  and  $P_{\Theta\Theta}$  are known, then distance measures will be determined precisely through this orthogonality. It is very interesting to note that there is indeed a way to probe perpendicular and parallel distance measures separately.

In practice,  $\tilde{P}$  is not observed in true coordinate frame but in reference frame. The following transformation is obtained,

$$\tilde{P}(k_{\text{ref}}, \mu_{\text{ref}}; z) / V_{\text{ref}} = \tilde{P}(k, \mu; z) / V \quad (4)$$

where  $V$  is a volume factor given by  $V = D_A^2 H^{-1}$ . If we define projected spectra  $\mathcal{P}$  as,

$$\mathcal{P}(k, \mu, z) \equiv \tilde{P}(k, \mu, z) [V_{\text{ref}}(z) / V(z)], \quad (5)$$

then logarithmic derivatives of  $\mathcal{P}$  in terms of  $D_A$  and  $H^{-1}$  are given by,

$$\frac{d \ln \mathcal{P}(k, \mu)}{d \ln D_A} = \frac{d \ln \tilde{P}(k, \mu)}{d \ln D_A} - 2 \quad (6)$$

$$\frac{d \ln \mathcal{P}(k, \mu)}{d \ln H^{-1}} = \frac{d \ln \tilde{P}(k, \mu)}{d \ln H^{-1}} - 1. \quad (7)$$

Constants in the above equations represent the volume factor effects. If those effects dominate, then orthogonal feature of  $D_A$  and  $H^{-1}$  will be wiped out. We present results in the bottom panel of Fig. 1. Although it becomes degenerate at  $\mu \rightarrow 0$ , distinct feature remains at  $\mu \rightarrow 1$ , which enables us to decompose  $D_A$  and  $H^{-1}$  in still good precision. Hereafter, this volume factor is included in the derivatives of  $\tilde{P}$ .

We investigate detectability of  $D_A$  and  $H^{-1}$  in this subsection, when  $P_{gg}$  and  $P_{\Theta\Theta}$  are fixed. In general, those spectra are unknown. If  $P_{gg}$  and  $P_{\Theta\Theta}$  float as well, additional degeneracies arise between  $D_A$  and  $P_{gg}$  at  $\mu \rightarrow 0$ , and between  $H^{-1}$  and  $P_{\Theta\Theta}$  at  $\mu \rightarrow 1$ . In the following subsections, we introduce approaches to break full degeneracies among all observables.

### C. Estimation to derive detectability

We estimate errors to decompose those all components introduced in the previous subsection using the following Fisher matrix analysis [23]. With the consideration of the non-perturbative contribution and the perfect correlation between  $g$  and  $\Theta$  at linear regime, the power spectra in redshift space,  $\tilde{P}$  in Eq. 1, are rewritten as [51],

$$\begin{aligned} \tilde{P}(k, \mu, z) &= \{P_{gg}(k, z) + 2\mu^2 r(k) [P_{gg}(k, z) P_{\Theta\Theta}(k, z)]^{1/2} \\ &+ \mu^4 P_{\Theta\Theta}(k, z)\} G_{\text{FoG}}(k, \mu, \sigma_z). \end{aligned} \quad (8)$$

The cross-correlation coefficient  $r(k)$  is defined as  $r(k) \equiv P_{g\Theta} / \sqrt{P_{gg} P_{\Theta\Theta}}$ . The density-velocity fields are highly

correlated for  $k < 0.1 h \text{Mpc}^{-1}$  thus we assume that the density and velocities are perfectly correlated,  $r(k) \sim 1$ . The density-velocity cross-spectra become the geometric mean of the two auto-spectra to leave only two free functions,  $P_{gg}$  and  $P_{\Theta\Theta}$ . Uncertainty in the observed redshifts is modeled by a line-of-sight smearing effect of the structure using fitting function  $G_{\text{FoG}} = e^{-k^2 \sigma_z^2 \mu^2}$  where  $\sigma_z$  denotes one-dimensional velocity dispersion (FoG: Finger-of-God effect) [30, 50–53]. For simplicity, we set  $G_{\text{FoG}} = 1$  in this work.

Errors of determining parameter  $p_\alpha$  out of  $\tilde{P}$  can be estimated using Fisher matrix analysis determining the sensitivity of a particular measurement. Fisher matrix for this decomposition,  $F_{\alpha\beta}^{\text{dec}}$ , is written as,

$$F_{\alpha\beta}^{\text{dec}} = \int \frac{\partial \tilde{P}(\vec{k})}{\partial p_\alpha} \frac{V_{\text{eff}}(\tilde{P})}{\tilde{P}(\vec{k})^2} \frac{\partial \tilde{P}(\vec{k})}{\partial p_\beta} \frac{d^3 k}{2(2\pi)^3}. \quad (9)$$

The effective volume  $V_{\text{eff}}(\tilde{P})$  is given by,

$$V_{\text{eff}}(\tilde{P}) = \left[ \frac{n\tilde{P}}{n\tilde{P} + 1} \right]^2 V_{\text{survey}}, \quad (10)$$

where  $n$  denotes galaxy number density, here  $n = 5 \times 10^{-3} (h^{-1} \text{Mpc})^{-3}$ . Comoving volume,  $V_{\text{survey}}$ , given by each redshift shell from  $z = 0$  to  $2$  with  $\Delta z = 0.2$  ( $f_{\text{sky}} = 1/2$ ) is written as,

$$V_{\text{survey}} = f_{\text{sky}} \frac{4\pi}{3} (D_{\text{outer}}^3 - D_{\text{inner}}^3), \quad (11)$$

where  $D_{\text{outer}}$  and  $D_{\text{inner}}$  denote comoving distances of outer and inner shell of the given redshift bin respectively. Theoretical estimation of density-density and velocity-velocity spectra using this method is studied in [23].

#### D. Approach I: shape of spectra prior

In this subsection, we present an easier approach to determine distance measures. Although full information of spectra are unknown,  $D_A$  and  $H^{-1}$  are observable with given shape of spectra.

The shape of the power spectra of density-density and velocity-velocity correlations critically depends on the epoch of matter-radiation equality. Under the paradigm of inflationary theory, initial fluctuations are stretched outside the horizon at different epochs which generates the tilt in the power spectrum. The predicted initial tilting is parameterised as a spectral index ( $n_S$ ) which is just the shape dependence due to the initial conditions. When the initial fluctuations reach the coherent evolution epoch after matter-radiation equality, they experience a scale-dependent shift from the moment they re-enter the horizon to the equality epoch. Gravitational instability is governed by the interplay between radiative pressure resistance and gravitational infall. The different duration of modes during this period result in a secondary shape dependence in the power spectrum. This shape dependence is determined by the ratio between matter

and radiation energy densities and sets the location of the matter-radiation equality in the time coordinate [54]. Therefore, the broadband shape is well determined, in a model-independent way, when the shape parameters of  $n_S$ ,  $\omega_m$  and  $\omega_b$  are given [42].

Assuming that linear theory holds, the parameter set  $p_\alpha$  is given by  $(G_g(z_j), G_\Theta(z_j), D_A(z_j), H^{-1}(z_j), \omega_m, \omega_b, n_S)$ . Here  $G_X$  denotes the coherent growth factor defined by,

$$\begin{aligned} P_{\Phi\Phi}(k, a) &= Q_\Phi(k) G_\Phi^2(a), \\ P_{gg}(k, a) &= Q_m(k) G_g^2(a), \\ P_{\Theta\Theta}(k, a) &= Q_m(k) G_\Theta^2(a), \end{aligned} \quad (12)$$

where the subscript  $\Phi$  denotes the curvature perturbation in the Newtonian gauge,

$$ds^2 = -(1 + 2\Psi)dt^2 + a^2(1 + 2\Phi)dx^2. \quad (13)$$

The growth function  $G_g$  is defined as  $G_g \equiv b\delta_m$  where  $b$  is the standard linear bias parameter between the density of galaxies and the underlying dark matter,  $\delta_m$ . As we follow the positive sign conversion,  $G_\Theta$  is the growth function of  $-\Theta$ . We further assume the scale independent bias at scales  $k < 0.1 h \text{Mpc}^{-1}$ . The shape factor of the perturbed metric power spectra  $Q_\Phi(k)$  is defined as

$$Q_\Phi(k) = \frac{2\pi^2}{k^3} \frac{9}{25} \Delta_{\zeta_0}^2(k) T_\Phi^2(k), \quad (14)$$

which is a dimensionless metric power spectra at  $a_{eq}$  (the matter-radiation equilibrium epoch), and  $\Delta_{\zeta_0}^2(k)$  is the initial fluctuations in the comoving gauge and  $T_\Phi(k)$  is the transfer function normalised at  $T_\Phi(k \rightarrow 0) = 1$ . The primordial shape  $\Delta_{\zeta_0}^2(k)$  depends on  $n_S$  (the slope of the primordial power spectrum), as  $\Delta_{\zeta_0}^2(k) = A_S^2(k/k_p)^{n_S - 1}$ , where  $A_S^2$  is the amplitude of the initial comoving fluctuations at the pivot scale,  $k_p = 0.002 \text{ Mpc}^{-1}$ . The intermediate shape factor  $T_\Phi(k)$  depends on  $\omega_m$ .

The shape factor for the matter fluctuations,  $Q_m(k)$ , which is important for both the galaxy-galaxy and velocity-velocity power spectra in Eq. 12 above, is given by the conversion from  $Q_\Phi(k)$  of,

$$Q_m(k) \equiv \frac{4}{9} \frac{k^4}{H_0^4 \Omega_m^2} Q_\Phi(k), \quad (15)$$

where, assuming  $c = 1$ , we can write  $H_0 \equiv 1/2997 h \text{Mpc}^{-1}$ .

Derivatives in Fisher matrix in terms of  $(G_g(z_j), G_\Theta(z_j))$  are given by,

$$\begin{aligned} \frac{\partial \ln \tilde{P}(k, \mu, z_j)}{\partial G_g(z_j)} &= \frac{2Q_m(k)}{\tilde{P}(k, \mu, z_j)} [G_g(z_j) + \mu^2 G_\Theta(z_j)] \\ \frac{\partial \ln \tilde{P}(k, \mu, z_j)}{\partial G_\Theta(z_j)} &= \frac{2\mu^2 Q_m(k)}{\tilde{P}(k, \mu, z_j)} [G_g(z_j) + \mu^2 G_\Theta(z_j)] \end{aligned} \quad (16)$$

and derivatives in terms of  $(D_A(z_j), H^{-1}(z_j))$  are given by,

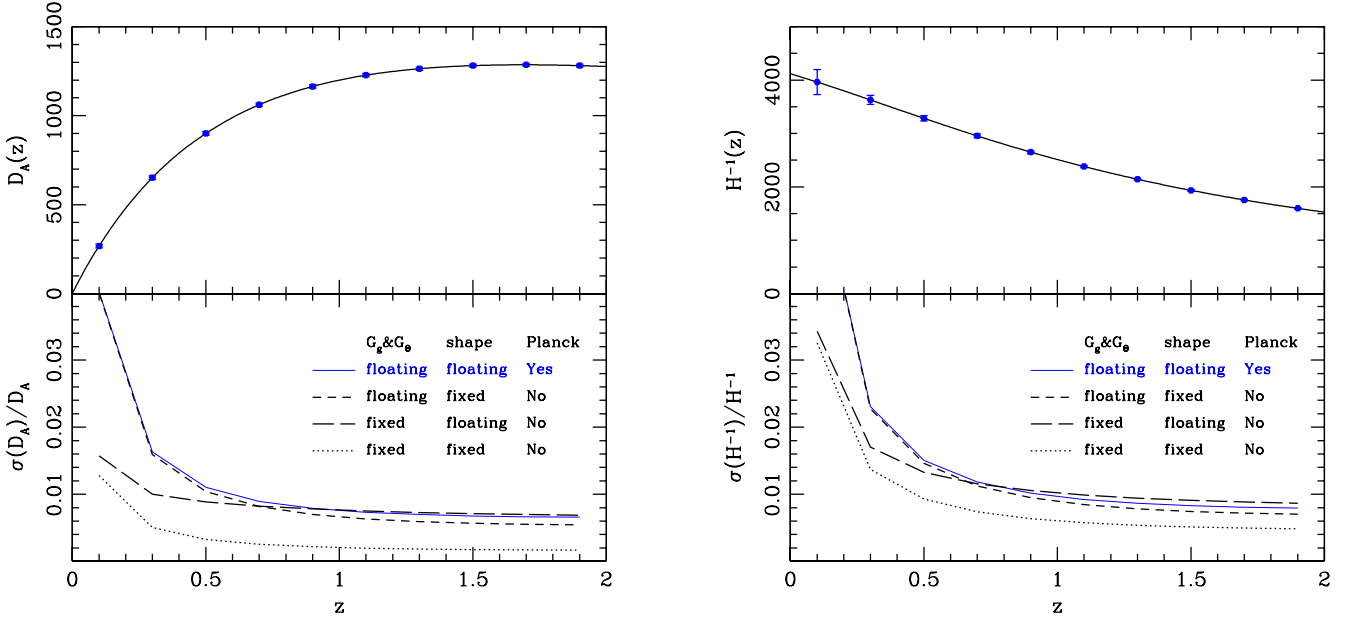


FIG. 2: (Left panel) The fiducial  $D_A(z)$  is presented as black curve in the top panel. Cases for the fractional errors are presented in the bottom panel; dotted curve (fixed  $G_g$  &  $G_\Theta$ , fixed shape of spectra, no Planck prior), dash curve (floating  $G_g$  &  $G_\Theta$ , fixed shape of spectra, no Planck prior), long dash curve (fixed  $G_g$  &  $G_\Theta$ , floating shape of spectra, no Planck prior), and thin solid curve (floating  $G_g$  &  $G_\Theta$ , floating shape of spectra, applying Planck prior). (Right panel) The same captions for  $H^{-1}$  as in the left panel.

$$\begin{aligned} \frac{\partial \ln \tilde{P}(k, \mu, z_j)}{\partial \ln D_A(z_j)} &= \frac{1}{\tilde{P}(k, \mu, z_j)} \left[ \frac{\partial \tilde{P}(k, \mu, z_j)}{\partial \ln k} \frac{\partial \ln k}{\partial \ln D_A(z_j)} + \frac{\partial \tilde{P}(k, \mu, z_j)}{\partial \ln \mu} \frac{\partial \ln \mu}{\partial \ln D_A(z_j)} \right] \\ \frac{\partial \ln \tilde{P}(k, \mu, z_j)}{\partial \ln H^{-1}(z_j)} &= \frac{1}{\tilde{P}(k, \mu, z_j)} \left[ \frac{\partial \tilde{P}(k, \mu, z_j)}{\partial \ln k} \frac{\partial \ln k}{\partial \ln H^{-1}(z_j)} + \frac{\partial \tilde{P}(k, \mu, z_j)}{\partial \ln \mu} \frac{\partial \ln \mu}{\partial \ln H^{-1}(z_j)} \right], \end{aligned} \quad (17)$$

where,

$$\begin{aligned} \frac{\partial \ln k}{\partial \ln D_A} &= -(1 - \mu^2) \\ \frac{\partial \ln \mu}{\partial \ln D_A} &= (1 - \mu^2) \\ \frac{\partial \ln k}{\partial \ln H^{-1}} &= -\mu^2 \\ \frac{\partial \ln \mu}{\partial \ln H^{-1}} &= -(1 - \mu^2). \end{aligned} \quad (18)$$

Fisher matrix components with the variation of  $(\omega_m, \omega_b, n_S)$  are calculated computationally using CAMB output.

We present the detectability of distance measures. Dotted curves in the bottom panels of Fig. 2 represent errors when fixing both growth functions and shape of spectra. Both  $D_A$  and  $H^{-1}$  are well measured at a sub-percentage accuracy.

We investigate the effects of the unknown overall amplitudes of growth functions and shape of spectra. Dash curves in Fig. 2 represent detectability to float growth

functions with the fixed shape of spectra. It shows weakened constraints on  $D_A$  and  $H^{-1}$  by a factor of 3 and 1.5 respectively. Next, we float the shape spectra with the fixed growth functions. Long dash curves in Fig. 2 represent constraints on  $D_A$  and  $H^{-1}$  weakened by a factor of 3 and 2 respectively. Finally, when we float both growth functions and shape of spectra, constraints on  $D_A$  and  $H^{-1}$  are blown by a factor of 10. In reality, we do not know either growth functions nor shape of spectra.

This blown-off detectability is commonly improved by a combination with other experiments such as CMB. In practice, we are not able to fix the shape parameters. We float those shape parameters, and marginalize with CMB experiments. For the CMB power spectra marginalization, we include in our analysis the unlensed  $C_l$  spectra of temperature–temperature, temperature–polarization and polarization–polarization and use the expected errors for Planck survey. This treatment is nearly equivalent to using distance information measured by CMB. We list diagonal elements of CMB prior information used for prior;  $\sigma(\omega_m) = 4.9 \times 10^{-4}$ ,  $\sigma(\omega_b) = 3.7 \times 10^{-5}$ ,

$\sigma(n_S) = 1.7 \times 10^{-3}$ . Estimated errors are shown as thin blue solid curves in the bottom panels of Fig. 2. Thin blue solid curves approach to dash curves which are the case of floating distance measures and fixed shape of spectra. Planck prior resolves uncertainties caused by unknown shape of spectra. The error bars shown in the top panels of Fig. 2 are estimated using Planck prior.

### E. Approach II: FLRW prior

In this subsection, we investigate an alternative method to probe distance measures using redshift survey alone without an assistance of other experiments like Planck in the previous subsection. Mathematical description of our universe is possible by assuming the cosmological principle. Our understanding of the perturbation theory is based upon the spartial homogeneity of the universe. In homogenous FLRW universe, the perpendicular component of distance measures are expressed by parallel component of Hubble flow. The angular diameter distance represents the perpendicular component, and it is expressed by the integrated sum of Hubble flow from the current to the targeted epochs. Therefore, if the wide-deep field survey is designed to be fully tomographic through all redshift spaces, then both different components of distance measures can be unified.

With suggested tomographical wide-deep field survey design, the angular diameter distance of  $D_A$  is approximately expressed by discrete sum of Hubble flow of  $H^{-1}$  at each redshift bin as,

$$D_A(z_j) = \frac{1}{1+z_j} \int_0^{z_j} dz' H^{-1}(z') \sim \frac{1}{1+z_j} \sum_{j'=1}^{N_j} H^{-1}(z_{j'}) \Delta z_{j'}, \quad (19)$$

where  $N_j$  represents the total number of redshift bins up to the targeted redshift of  $z_j$ . Then  $p_\alpha$  parameter space for distance measures is unified into a single parameter of Hubble flow  $H^{-1}$ . Most future spectroscopy wide-deep field redshift survey programs such as SUBARU PFS, BigBOSS and EUCLID are planned to make full tomographic scanning [55–57]. The parameter set of  $p_\alpha$  becomes  $(G_g(z_j), G_\Theta(z_j), H^{-1}(z_j'), \omega_m, \omega_b, n_S)$ . The derivatives in terms of  $(P_{gg}(k_i, z_j), \tilde{P}_{\Theta\Theta}(k_i, z_j))$  are given in Eq. 24, and the derivative in terms of  $H^{-1}(z_j)$  is given by,

$$\frac{\partial \ln \tilde{P}(k, \mu, z_j)}{\partial \ln H^{-1}(z_j')} = \frac{1}{\tilde{P}(k, \mu, z_j)} \frac{\partial \tilde{P}(k, \mu, z_j)}{\partial \ln k} \frac{\partial \ln k}{\partial \ln H^{-1}(z_j')} + \frac{1}{\tilde{P}(k, \mu, z_j)} \frac{\partial \tilde{P}(k, \mu, z_j)}{\partial \ln \mu} \frac{\partial \ln \mu}{\partial \ln H^{-1}(z_j')}$$

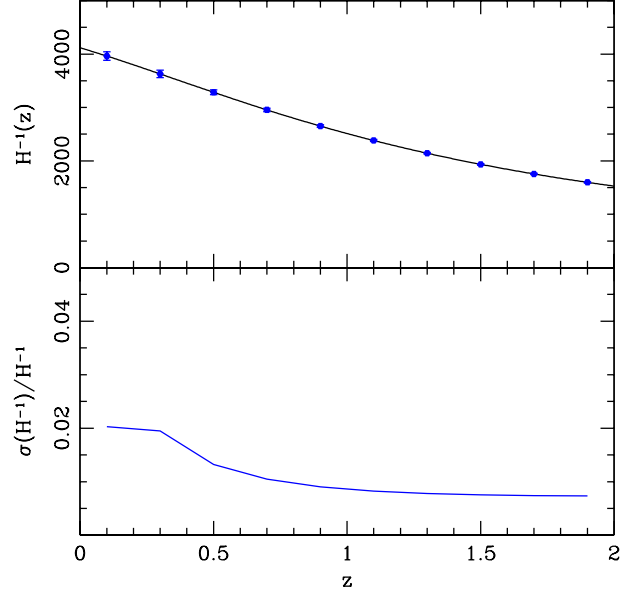


FIG. 3: Black solid curve in the top panel represents fiducial  $H^{-1}(z)$  with error bars estimated using FLRW prior in small curvature approximation. Blue solid curve in the bottom panel represents fractional errors.

where

$$\begin{aligned} \frac{\partial \ln k}{\partial \ln H^{-1}(z_{j'})} &= \frac{\partial \ln k}{\partial \ln D_A(z_j)} \frac{\partial \ln D_A(z_j)}{\partial \ln H^{-1}(z_{j'})} - \mu^2 \delta_{jj'} \quad (20) \\ \frac{\partial \ln \mu}{\partial \ln H^{-1}(z_{j'})} &= \frac{\partial \ln \mu}{\partial \ln D_A(z_j)} \frac{\partial \ln D_A(z_j)}{\partial \ln H^{-1}(z_{j'})} - (1 - \mu^2) \delta_{jj'}, \end{aligned}$$

where  $z_{j'} < z_j$  and  $\delta_{jj'} = 1$  at  $j = j'$  otherwise 0. The reduction of parameter space for distance measures enhances the detectability of  $p_\alpha$  parameter.

In Fig. 3, we present the detectability of Hubble flow from  $z = 0.1$  to  $z = 1.9$ . Solid curve in the bottom panel represents the achievable precision level. Due to volume limit, the detectability is slightly over 1% accuracy at  $z < 0.5$ . But at the redshift bins of  $z > 0.5$ ,  $H^{-1}$  is measured much better than 1% accuracy. There are many observational methods to probe Hubble flow using cosmological parameters, but none of those probe Hubble flow in theoretical model independent way. Although the Hubble flow  $H_0$  at current epoch can be measured directly using distance ladder, the full evolution of  $H$  has yet been attempted to be measured in this precision.

In addition to this, it is interesting to observe the self-determination of shape factors with Friedman prior. Even without Planck combined, we achieve the following constraints on shape parameters;  $\sigma(\omega_m) = 1.1 \times 10^{-3}$ ,  $\sigma(\omega_b) = 5.8 \times 10^{-4}$ ,  $\sigma(n_S) = 5.9 \times 10^{-3}$ . It suggests that full non-parameteric reconstruction of spectra is possible, which is discussed in next section in detail.

The expression in Eq. 19 is not applicable for the case of curved space-time. This implicit flat universe prior can be lifted off easily. We define curvature parameter  $\mathcal{K}$

as,

$$\mathcal{K} = \sqrt{|\Omega_k| h^2} / 2997.2 h \text{ Mpc}^{-1}. \quad (21)$$

Then parameter space of  $p_\alpha$  is extended into  $(G_g(z_j), G_\Theta(z_j), H^{-1}(z'_j), \omega_m, \omega_b, n_S, \mathcal{K})$ . The estimated angular diameter distance  $D_A(z_j)$  is given with open curvature as,

$$D_A(z_j) = \frac{1}{\mathcal{K}(1+z_j)} \sinh \left[ \mathcal{K} \sum_{j'=1}^{N_j} H^{-1}(z_{j'}) \Delta z_{j'} \right], \quad (22)$$

and with closed curvature as,

$$D_A(z_j) = \frac{1}{\mathcal{K}(1+z_j)} \sin \left[ \mathcal{K} \sum_{j'=1}^{N_j} H^{-1}(z_{j'}) \Delta z_{j'} \right]. \quad (23)$$

We investigate impact on the detectability from added curvature degree of freedom. We find that constraints on  $H^{-1}(z_j)$  becomes poorer by a factor of 1.5 with curvature marginalization.

However, constraints on curvature of the space have been nailed down to the vicinity about flatness. Even though the space is curved, it is likely to be a couple of percentage deviation from flatness, which is consistent with prediction of inflationary paradigm as well. In this small curvature approximation of  $\mathcal{K} \ll 1$ ,  $D_A$  can be approximately given by Eq. 19 in our interest redshift range of  $z < 2$ . From now, when we mention FLRW prior, this small curvature approximation is applied.

### III. CHALLENGE TO MEASURE SPECTRA IN MODEL INDEPENDENT WAY

We present the detectability of growth functions of  $G_g$  and  $G_\Theta$  in Fig. 4. The detectability of  $G_g$  and  $G_\Theta$  is studied in detail [23], when both distance measures and shape of spectra are fixed. Dotted curves in the bottom panels of Fig. 4 reproduce well the previous results. First, we test the impact of floating distance measures on errors represented by dotted curves. Dash curves in Fig. 4 represent fractional errors when floating  $D_A$  and  $H^{-1}$ . The detectability of  $G_g$  and  $G_\Theta$  is weakened by a factor of 3 and 1.5 respectively. Second, we test the impact of floating shape parameters on errors represented by dotted curves. Long dash curves in Fig. 4 represent those results. If distance measures are fixed, growth functions and shape parameters are determined in good precision even without combination of CMB experiments. Finally, we float both distance measures and shape of spectra. None of  $G_g$  and  $G_\Theta$  are measured in precision. Constraints on  $G_g$  and  $G_\Theta$  become much worse.

We generalize parameterization of growth functions and shape of spectra with Fourier modes of power spectra. Fourier space is binned into 20 bins from 0.005  $h^{-1} \text{ Mpc}$  to 0.105  $h^{-1} \text{ Mpc}$ . The full set of parameter

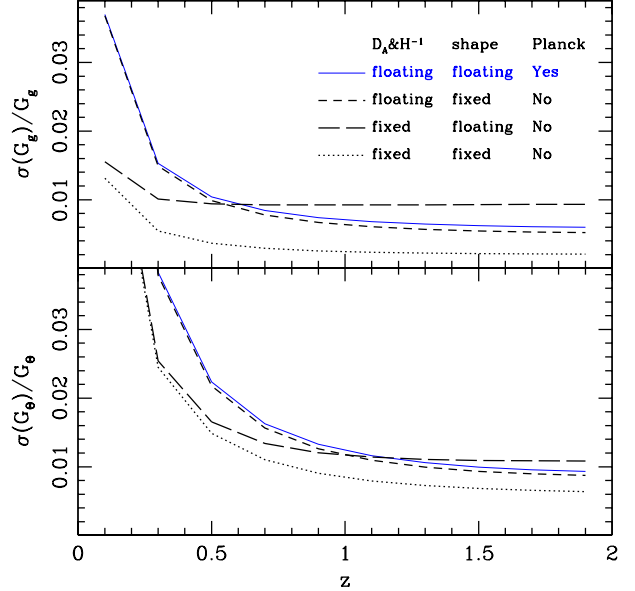


FIG. 4: (Top panel) Cases for the fractional errors are presented; dotted curve (fixed  $D_A$  &  $H^{-1}$ , fixed shape of spectra, no Planck prior), dash curve (floating  $D_A$  &  $H^{-1}$ , fixed shape of spectra, no Planck prior), long dash curve (fixed  $D_A$  &  $H^{-1}$ , floating shape of spectra, no Planck prior), and thin solid curve (floating  $D_A$  &  $H^{-1}$ , floating shape of spectra, applying Planck prior). (Bottom panel) The same captions for  $G_\Theta$  as in the top panel.

space of  $p_\alpha$  becomes  $(P_{gg}(k_i, z_j), P_{\Theta\Theta}(k_i, z_j), D_A(z_j), H^{-1}(z_j))$ . The subscript “ $i$ ” denotes 20  $k$  bins, and the subscript “ $j$ ” denotes 10  $z$  bins from 0 to 2. Variation of  $(P_{gg}(k_i, z_j), P_{\Theta\Theta}(k_i, z_j))$  represents simultaneous floatation of growth functions and shape of spectra. This approach has advantage for an exotic dark energy or modified gravity model in which growth functions become scale dependent [46, 47].

The derivatives in terms of  $(P_{gg}(k_i, z_j), P_{\Theta\Theta}(k_i, z_j))$  in Fisher matrix are given by,

$$\begin{aligned} \frac{\partial \ln \tilde{P}(k, \mu, z_j)}{\partial P_{gg}^{\text{dec}}(k_i, z_j)} &= \frac{\Theta_i(k)}{\tilde{P}(k, \mu, z_j)} \left[ 1 + \mu^2 \sqrt{\frac{P_{\Theta\Theta}(k_i, z_j)}{P_{gg}(k_i, z_j)}} \right] \\ \frac{\partial \ln \tilde{P}(k_i, \mu, z_j)}{\partial P_{\Theta\Theta}^{\text{dec}}(k_i, z_j)} &= \frac{\mu^2 \Theta_i(k)}{\tilde{P}(k_i, \mu, z_j)} \left[ \sqrt{\frac{P_{gg}(k_i, z_j)}{P_{\Theta\Theta}(k_i, z_j)}} + \mu^2 \right], \end{aligned} \quad (24)$$

where  $\Theta_i(k)$  denotes step function in which  $\Theta_i(k) = 1$  at  $k$  belong to  $k_i$  bin, otherwise  $\Theta_i(k) = 0$ . The derivative terms of distance measures are the same as in Eq. 17. The shape factor floats intrinsically in this general parameterization. If distance measures float as well, none of spectra are measured precisely. If one wants to measure fluctuations of  $(P_{gg}, P_{\Theta\Theta})$ , then distance measures should be provided by other experiments such as supernovae.

In this section, we investigate a new method to probe spectra using redshift survey alone without an assistance

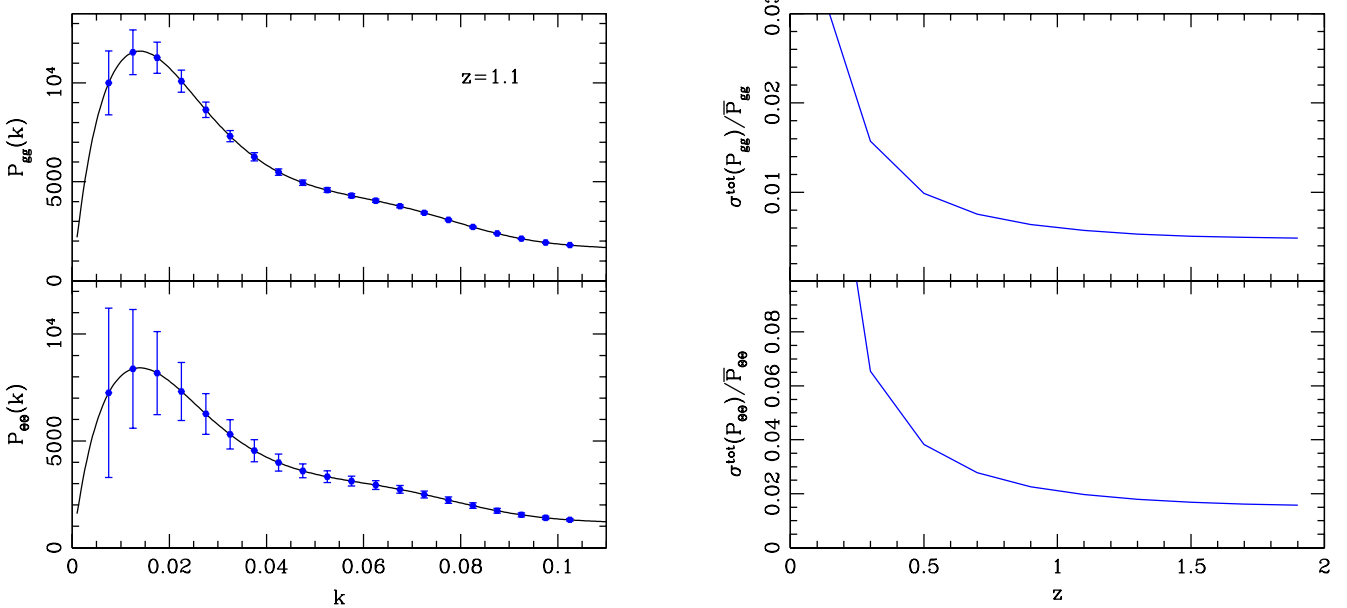


FIG. 5: (Left panel) Spectra at  $z = 1.1$  are presented. Solid curve in the top panel represents fiducial  $P_{gg}(k)$ , and solid curve in the bottom panel represents  $P_{\Theta\Theta}(k)$ . Error bars on the curves represent theoretical estimation using FLRW prior. (Right panel) Summed fractional errors of spectra at each given redshift are presented with applying FLRW prior.

of other experiments. With FLRW prior, the set of parameter space of  $p_\alpha$  becomes  $(P_{gg}(k_i, z_j), P_{\Theta\Theta}(k_i, z_j), H^{-1}(z_j))$ . Constraints on power spectra of  $P_{gg}(k_i, z_j)$  and  $P_{\Theta\Theta}(k_i, z_j)$  with fixed distance measures are studied in detail [23]. The previous results are updated by floating distance measures with applying Friedman universe prior. In the left panel of Fig. 5, solid curves in the top and bottom panels represent fiducial  $P_{gg}(k_i, z_j = 1.1)$  and  $P_{\Theta\Theta}(k_i, z_j = 1.1)$ , and error bars on the curves are estimated using FLRW prior. When FLRW prior is applied, the measured power spectra with floating distance measures are probed as precise as the measured power spectra with fixed distance measures.

We continue our test at the other redshift bins. Here we present the results using cumulated error of  $\sigma^{\text{tot}}(P)$  which is given by,

$$[\sigma^{\text{tot}}(P)]^{-2} = \sum_{i,j=i_{k_{\min}}}^{i_{k_{\max}}} P(k_i) C^{-1}[P(k_i), P(k_j)] P(k_j) \quad (25)$$

where  $C^{-1}$  is the inverse of covariance matrix calculated using Fisher matrix. In the top right panel of Fig. 5,  $\sigma^{\text{tot}}(P_{gg})$  is presented from  $z = 0.1$  to  $z = 1.9$ . The precision to measure  $P_{gg}(k_i, z_j)$  is not weakened through all redshifts. In the bottom right panel of Fig. 5, summed errors for  $P_{\Theta\Theta}(k_i, z_j)$  are presented. Again, power spectra of coherent motions are well measured even after marginalizing distance measures.

We have to explain the reason why the degeneracy among the parameters are broken, even though principal components approach is used for spectra. The spectra are not principally parameterized along  $\mu$  direction. Spectra

$P_{gg}(k_i, z_j)$  are uniquely determined at  $\mu$  bins approaching  $\mu \rightarrow 0$ , while  $P_{\Theta\Theta}(k_i, z_j)$  are mainly determined at  $\mu$  bins approaching  $\mu \rightarrow 1$ . However, the impact of parameterized  $H$  does not pivot at  $\mu \rightarrow 0$  limit nor  $\mu \rightarrow 1$  limit, but prevails through  $\mu$  bins in coherent way. It breaks the degeneracy among parameters.

#### IV. DISCUSSION

If we float freely both the spectra of  $P_{gg}$  and  $P_{\Theta\Theta}$  and the distance measures of  $D_A$  and  $H^{-1}$ , then we are incapable of providing any observable out of galaxy distributions in redshift space. It has been underestimated the significance of this degeneracy between fluctuations and distance measures. Unless distance measures of  $D_A$  and  $H^{-1}$  are given by other experiments, there is no observation of fluctuations. Unless any piece of information about fluctuations is known, there is no probe of distance measures. Specific conditions on either component should be imposed to make targeted observation.

We investigate the detectability of parameter  $p_\alpha$  with a given broadband shape of spectra. In this manuscript, the broadband shape is given by a few shape cosmological parameters of  $(\omega_m, \omega_b, n_S)$ , instead of phenomenological parameters. The primordial shape during inflation is determined by  $n_S$ , and the transferred shape before matter-radiation equality epoch is described by  $\omega_m$  and  $\omega_b$ . The scale dependence of spectra of  $P_{gg}$  and  $P_{\Theta\Theta}$  is dropped off to leave only the time dependent factors parameterized by growth functions of  $G_g$  and  $G_\Theta$ . Tight constraints on  $(G_g, G_\Theta, D_A, H^{-1})$  are expected when

the shape parameters are marginalized with CMB experiments. However, if CMB experiments marginalization is lifted off, the detectability gets worse by a factor of 10. There are some classes of theoretical models in which the shape of spectra is not fully determined at last scattering surface. Then there will be no precise observables despite the given broadband shape of spectra, as far as no external priors on the shape of spectra are provided. The degeneracy between fluctuations and distance measures still prevails with the condition of given broadband shape of spectra.

We propose new treatment to extract observables with assuming a minimal theoretical ansatz. Our standard model of perturbation theory is based upon the cosmological principle implying spartial homogeneity of the universe. It also leads us to unify two distinct components of distance measures into a single one with no additional theoretical prior. The perpendicular component of distance measures is represented by angular diameter distance which is an integrated sum of parallel component represented by Hubble flow. This reduction is possible by demanding an experimental design of wide-deep field redshift survey to be fully tomographic through all redshifts. We find that  $P_{gg}$ ,  $P_{\Theta\Theta}$  and  $H^{-1}$  are measured in precision about a sub-percentage level using this reduction of distance measure parameters only assuming the FLRW universe available.

It is remarkable that Hubble flow is measured in high precision at all redshifts shown in the right panel of Fig. 5. The direct measurement of Hubble flow is a key information to understand the history of the universe. The discovery of cosmic acceleration demands us to probe Hubble flow in a model independent way, because we lose confidence of the detailed matter-energy components of the universe or the validation of general relativity at cosmological scales. Direct measurement of  $H$  is possible by

distance ladder technique, but only at the local universe. There are other geometric probes developed, but indirectly measured by luminosity or angular diameter distances. But our method to probe Hubble flow is not only providing  $H$  measurements through all redshifts, but also independent of specific cosmological parameters. Redshift survey will reveal tomographic evolution of Hubble flow from the current to any targeted epoch as far as it is reached by spectroscopic survey. We also show that detectability of  $P_{\Theta\Theta}$  and  $H^{-1}$  is influenced by uncertainty of curvature, but it is not much severe in small curvature approximation.

However, we have to mention caveats. As it is well known, redshift distortion map is severely contaminated by non-linear smearing effect. It is indeed troublesome to decompose linear information out of this mixture. But there are many reports having been made for the possible precise decomposition of fluctuations with fixed distance measures. The contaminated maps can be decomposed into linear theory of spectra and non-smearing effect contributions up to limited scales of  $k < 0.1 h \text{ Mpc}^{-1}$ . Then the similar control of non-linear effect might be available for the case of relaxing distance measure prior. In near future, we will be back to the following work to full reconstruction of fluctuations and distance measures.

## Acknowledgments

We thank Hee-Jong Seo for assistance to initiate this work and for substantial inputs in this manuscript. We thank Eric Linder for helpful discussions during a KITPC workshop. Numerical calculations were performed by using a high performance computing cluster in the Korea Astronomy and Space Science Institute.

---

[1] A. Friedman, *Zeitschrift fur Physik* **10**, 377-386 (1922).  
[2] E. R. Harrison, *Phys. Rev. D* **1**, 2726 (1970).  
[3] A. Einstein and W. de Sitter, *Proc. Nat. Acad. Sci.* **18**, 213 (1932).  
[4] A. G. Riess *et al.* [Supernova Search Team Collaboration], *Astron. J.* **116**, 1009 (1998) [astro-ph/9805201].  
[5] S. Perlmutter *et al.* [Supernova Cosmology Project Collaboration], *Astrophys. J.* **517**, 565 (1999) [astro-ph/9812133].  
[6] D. G. York *et al.* [SDSS Collaboration], *Astron. J.* **120**, 1579 (2000) [astro-ph/0006396].  
[7] J. A. Peacock, S. Cole, P. Norberg, C. M. Baugh, J. Bland-Hawthorn, T. Bridges, R. D. Cannon and M. Colless *et al.*, *Nature* **410**, 169 (2001) [astro-ph/0103143].  
[8] E. Hawkins, S. Maddox, S. Cole, D. Madgwick, P. Norberg, J. Peacock, I. Baldry and C. Baugh *et al.*, *Mon. Not. Roy. Astron. Soc.* **346**, 78 (2003) [astro-ph/0212375].  
[9] W. J. Percival *et al.* [2dFGRS Collaboration], *Mon. Not. Roy. Astron. Soc.* **353**, 1201 (2004) [astro-ph/0406513].  
[10] I. Zehavi *et al.* [SDSS Collaboration], *Astrophys. J.* **630**, 1 (2005) [astro-ph/0408569].  
[11] M. Tegmark *et al.* [SDSS Collaboration], *Phys. Rev. D* **74**, 123507 (2006) [astro-ph/0608632].  
[12] L. Guzzo, M. Pierleoni, B. Meneux, E. Branchini, O. L. Fevre, C. Marinoni, B. Garilli and J. Blaizot *et al.*, *Nature* **451**, 541 (2008) [arXiv:0802.1944 [astro-ph]].  
[13] M. J. Drinkwater, R. J. Jurek, C. Blake, D. Woods, K. A. Pimbblet, K. Glazebrook, R. Sharp and M. B. Pracy *et al.*, *Mon. Not. Roy. Astron. Soc.* **401**, 1429 (2010) [arXiv:0911.4246 [astro-ph.CO]].  
[14] E. A. Kazin *et al.* [SDSS Collaboration], *Astrophys. J.* **710**, 1444 (2010) [arXiv:0908.2598 [astro-ph.CO]].  
[15] B. A. Reid, W. J. Percival, D. J. Eisenstein, L. Verde, D. N. Spergel, R. A. Skibba, N. A. Bahcall and T. Budavari *et al.*, *Mon. Not. Roy. Astron. Soc.* **404**, 60 (2010) [arXiv:0907.1659 [astro-ph.CO]].  
[16] B. A. Reid, L. Samushia, M. White, W. J. Percival, M. Manera, N. Padmanabhan, A. J. Ross and

A. G. Sanchez *et al.*, arXiv:1203.6641 [astro-ph.CO].

[17] B. Jain and P. Zhang, Phys. Rev. D **78**, 063503 (2008) [arXiv:0709.2375 [astro-ph]].

[18] S. Nesseris and L. Perivolaropoulos, Phys. Rev. D **77**, 023504 (2008) [arXiv:0710.1092 [astro-ph]].

[19] Y. -S. Song and K. Koyama, JCAP **0901**, 048 (2009) [arXiv:0802.3897 [astro-ph]].

[20] Y. -S. Song and W. J. Percival, JCAP **0910**, 004 (2009) [arXiv:0807.0810 [astro-ph]].

[21] Y. Wang, JCAP **0805**, 021 (2008) [arXiv:0710.3885 [astro-ph]].

[22] W. J. Percival and M. White, arXiv:0808.0003 [astro-ph].

[23] M. White, Y. -S. Song and W. J. Percival, Mon. Not. Roy. Astron. Soc. **397**, 1348 (2008) [arXiv:0810.1518 [astro-ph]].

[24] P. McDonald and U. Seljak, JCAP **0910**, 007 (2009) [arXiv:0810.0323 [astro-ph]].

[25] Y. -S. Song and I. Kayo, Mon. Not. Roy. Astron. Soc. **407**, 1123 (2010) [arXiv:1003.2420 [astro-ph.CO]].

[26] J. Tang, I. Kayo and M. Takada, arXiv:1103.3614 [astro-ph.CO].

[27] D. Jeong and E. Komatsu, Astrophys. J. **651**, 619 (2006) [astro-ph/0604075].

[28] D. Jeong and E. Komatsu, Astrophys. J. **691**, 569 (2009) [arXiv:0805.2632 [astro-ph]].

[29] V. Desjacques and R. K. Sheth, Phys. Rev. D **81**, 023526 (2010) [arXiv:0909.4544 [astro-ph.CO]].

[30] A. Taruya, T. Nishimichi and S. Saito, Phys. Rev. D **82**, 063522 (2010) [arXiv:1006.0699 [astro-ph.CO]].

[31] E. Jennings, C. M. Baugh and S. Pascoli, Mon. Not. Roy. Astron. Soc. **410**, 2081 (2011) [arXiv:1003.4282 [astro-ph.CO]].

[32] B. A. Reid and M. White, arXiv:1105.4165 [astro-ph.CO].

[33] T. Okumura, U. Seljak, P. McDonald and V. Desjacques, JCAP **1202**, 010 (2012) [arXiv:1109.1609 [astro-ph.CO]].

[34] J. Kwan, G. F. Lewis and E. V. Linder, Astrophys. J. **748**, 78 (2012) [arXiv:1105.1194 [astro-ph.CO]].

[35] L. Samushia, W. J. Percival and A. Raccanelli, Mon. Not. Roy. Astron. Soc. **420**, 2102 (2012) [arXiv:1102.1014 [astro-ph.CO]].

[36] C. Blake, S. Brough, M. Colless, C. Contreras, W. Couch, S. Croom, T. Davis and M. J. Drinkwater *et al.*, Mon. Not. Roy. Astron. Soc. **415**, 2876 (2011) [arXiv:1104.2948 [astro-ph.CO]].

[37] P. Zhang, J. Pan and Y. Zheng, arXiv:1207.2722 [astro-ph.CO].

[38] E. Gaztanaga, A. Cabre and L. Hui, Mon. Not. Roy. Astron. Soc. **399**, 1663 (2009) [arXiv:0807.3551 [astro-ph]].

[39] C. Blake and K. Glazebrook, Astrophys. J. **594**, 665 (2003) [astro-ph/0301632].

[40] H. -J. Seo and D. J. Eisenstein, Astrophys. J. **598**, 720 (2003) [astro-ph/0307460].

[41] Y. Wang, Astrophys. J. **647**, 1 (2006) [astro-ph/0601163].

[42] Y. -S. Song, C. G. Sabiu, I. Kayo and R. C. Nichol, JCAP **1105**, 020 (2011) [arXiv:1006.4630 [astro-ph.CO]].

[43] C. -H. Chuang and Y. Wang, arXiv:1205.5573 [astro-ph.CO].

[44] F. Beutler, C. Blake, M. Colless, D. H. Jones, L. Staveley-Smith, G. B. Poole, L. Campbell and Q. Parker *et al.*, arXiv:1204.4725 [astro-ph.CO].

[45] C. Alcock and B. Paczynski, Nature **281**, 358 (1979).

[46] S. M. Carroll, V. Duvvuri, M. Trodden and M. S. Turner, Phys. Rev. D **70**, 043528 (2004) [astro-ph/0306438].

[47] G. R. Dvali, G. Gabadadze and M. Porrati, Phys. Lett. B **484**, 112 (2000) [hep-th/0002190].

[48] Y. -S. Song, W. Hu and I. Sawicki, Phys. Rev. D **75**, 044004 (2007) [astro-ph/0610532].

[49] N. Kaiser, Mon. Not. Roy. Astron. Soc. **227**, 1 (1987).

[50] K. B. Fisher, Astrophys. J. **448**, 494 (1995) [astro-ph/9412081].

[51] R. Scoccimarro, Phys. Rev. D **70**, 083007 (2004) [astro-ph/0407214].

[52] T. Matsubara, Phys. Rev. D **77**, 063530 (2008) [arXiv:0711.2521 [astro-ph]].

[53] M. Crocce and R. Scoccimarro, Phys. Rev. D **77**, 023533 (2008) [arXiv:0704.2783 [astro-ph]].

[54] D. J. Eisenstein and W. Hu, Astrophys. J. **496**, 605 (1998) [astro-ph/9709112].

[55] R. Ellis, M. Takada, H. Aihara, N. Arimoto, K. Bundy, M. Chiba, J. Cohen and O. Dore *et al.*, arXiv:1206.0737 [astro-ph.CO].

[56] D. Schlegel *et al.* [BigBOSS Collaboration], arXiv:1106.1706 [astro-ph.IM].

[57] A. Cimatti, R. Laureijs, B. Leibundgut, S. Lilly, R. Nichol, A. Reffregier, P. Rosati and M. Steinmetz *et al.*, arXiv:0912.0914 [astro-ph.CO].